Multiple Tab-and-Slot Joint : Improvement of the Rotational Stiffness for the Connection of Thin Structural Wood Panels

Stéphane Roche [1,2] **Julien Gamerro,**[2] **Yves Weinand**[2]

ABSTRACT: Researchers in Asia have focused on analyzing the rotational performance of traditional connections based on embedment. The Nuki through-joint has inspired work at the laboratory of wood construction (IBOIS), Ecole Polytechnique Fédérale de Lausanne, to improve the rotational behavior of the multiple tab and slot joint (MTSJ). In this work, through tenon (TT) and closed slot joints were added to initial dovetail and Nejiri arigata joints used for folded-plate structures. The bending performance of the improved MTSJ-TT joint was higher than that of screwed angular connections. Numerical monitoring of the embedded volumes under partial compression on the contact surfaces was used to characterize the directly and indirectly loaded areas. The decay coefficients for the exponential form, which defined the additional length in the indirectly loaded area, were quantified for both single (SC) and double contact (DC). The evolution of these coefficients was also monitored along the angular deformation. Finally, an analytical formulation of the embedded volumes was provided to prepare an analytical model for the MTSJ-TT joint subjected to bending.

KEYWORDS: timber, panel, through-connection, rotational embedment, multiple tab and slot joint.

1 INTRODUCTION

In 2014, Robeller described structural connections for thin engineered edge-joined wood panels [1]. The multi-edge in-situ connection of laminated veneer lumber (LVL) panels was demonstrated on a folded-plate prototype (Figure 1a), and a Yoshimura tessellation of trapezoidal plates was assembled with multiple tab-and-slot joints (MTSJs). Despite significant rigidity in rotation, the connections were weaker under bending than screws and adhesives [2].

At the same conference, Krieg et al. presented a pavilion that had a free-form geometry discretized with planar hexagonal meshes, which resulted in trivalent connections [3]. Except in the transition region between positive and negative Gaussian curvatures, where the plates approached a rectangle, the trivalent geometry resulted in bending stiffness despite each pair of connected edges being hinged. The mixed connection had finger joints bearing the in-plane shear forces and crossing screw joints bearing the axial and out-of-plane shear forces. In the transition zone, the screws provided the required bending stiffness.

Segmental plate shells with a trivalent geometry partially solved the bending stiffness, while a folded-plate structure improved the static height using thinner panels. For folded-plate structures (FPS), the rotational stiffness of the edge connection greatly affects the overall structural behavior.

Figure 1b shows a double layered FPS based on the Miura-ori pattern [4]. The connection of a maximum of two edges at a time made possible the in-plane insertion and the use of through tenon joints (TTs).

The embedment effect in a MTSJ with TT causes it to behave similarly to traditional Japanese through-joints in rotational partial compression. Researchers in Asia have studied the elasto-plastic rotational behavior of such joints [5][6][7], confirming their great rotational stiffness and ductility, which contributes to the stability of ancient structures, even during earthquakes. They based their models on embedment theory developed in Japan. Local compression loading produces directly and indirectly loaded areas. Inayama established an elastic formulation of this phenomenon for wood loaded perpendicular to the grain [8]. Tanahashi et al. derived the elasto-plastic embedment behavior of orthotropic wood analytically from the Pasternak soil model [9]. Tanahashi and Suzuki also worked on the rotational compression of the Nuki joint using this model [6]. Other works (e.g., Kitamori [10][11]) compared the additional length profile of the embedment areas for different contact cases (single/double, axial/rotational). Most of these works show that the indirectly loaded area is characterized by an exponential curve with a decay coefficient, γ (Equation 1).

$$f(x) = a \times \exp(-\gamma x) \tag{1}$$

Here, x is the abscissa on the non deformed surface and a is the maximum surface displacement. The coefficient γ defines the amplitude of the indirectly loaded area, and it varies according to the type of embedment and the material geometry and properties.

Inspired by the performance of Nuki joints in rotation, the present article examines the embedment behavior of TTs and closed slots that drastically improves the moment-

resisting performance of a MTSJ. The deformed volume is defined in the elastic and plastic range, and the decay coefficient is experimentally obtained for single contact (SC) and double contact (DC) with the grain parallel to the joint axis.
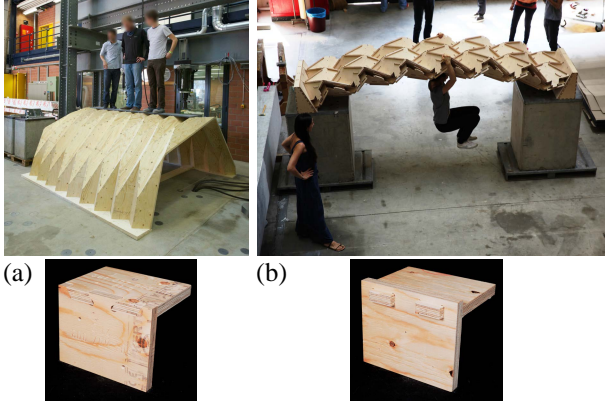

Figure 1: *(a) Yoshimura pattern and MTSJ (0°,0°,±30°), (b) Double-layer Miura-ori pattern and TTs.*

# 2 MTSJ DESIGN FOR IMPROVED ROTATIONAL STIFFNESS

The Nuki joint, a tie beam penetrating a mortise cut in a column, performs well as a moment-resisting connection. To improve the rotational stiffness of a MTSJ, a TT and closed slots were added to achieve a similar embedment effect to a Nuki joint under rotation. Eight geometries, including a MTSJ-TT, were tested to validate the improvement (Figure 2). The first group (samples (a) to (d)) has open slots. Sample (a) had the geometry of the sample that has been reported to provide the best compromise between stiffness in closing and opening [2]. The principle of the Nejiri arigata joint (MTSJ-JJ) is used with an insertion oriented by $\theta_1 = 0°, \theta_2 = 0°$ and a tab angle θ_3 equal to ±30° for the first and second half of the edge, respectively [1] [2]. Sample (b) is the MTSJ dovetail variante (DJ) of the same joint, and ±θ_3 is applied to each locking face. To limit kinematic slip during rotation, sample (c) was the same as sample (b) except it included one screw per tab, whereas sample (d) is a screwed MTSJ finger joint (FJ) alternative with $\theta_1, \theta_2, \theta_3 = 0°$. The next three samples (e, f, g) were designed with TTs and closed slots. Samples (e) and (f) had elastic tabs whose snap-fit (SF) function removed the last degree of freedom after insertion [12]. Sample (g) is a MTSJ with TTs (MTSJ-TT); the effect of embedment in in this joint is investigated in more detail in the following sections (Figure 3). For comparison, sample (h) was only connected with a screw on a butt joint.

3 BENDING EXPERIMENTS

Folding tests compared sample (g) in bending with the other configurations of MTSJ. Its performance is also rated with respect to screwed assemblies (Figure 2c,d,h).
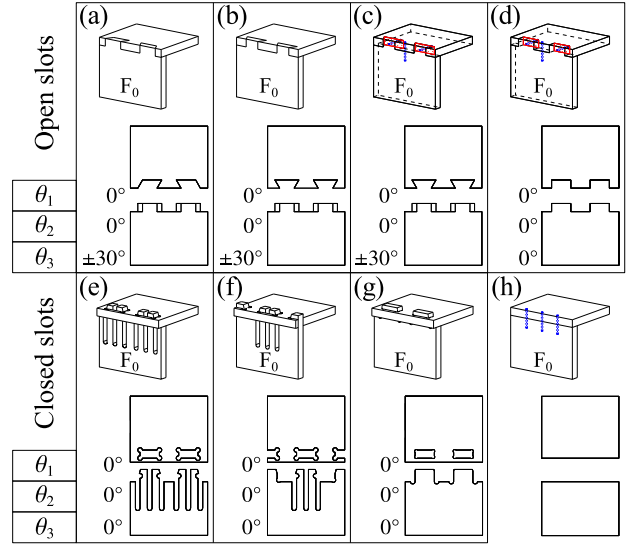

Figure 2: *MTSJ sample design.*
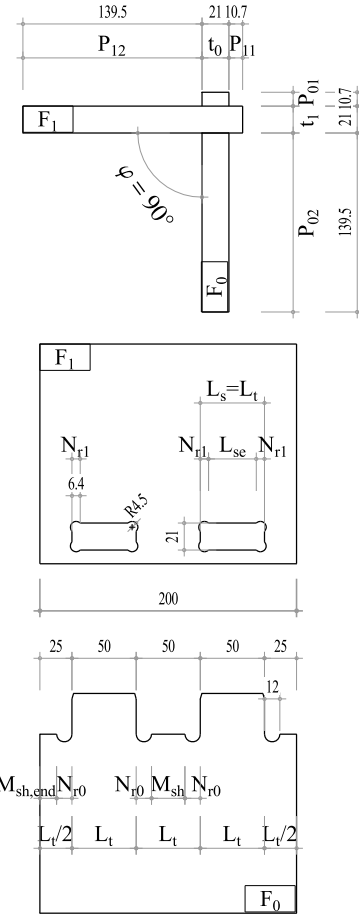
Figure 3: *Geometry of MTSJ with TTs.*

3.1 METHOD

The test setup was the same as that introduced by Roche et al. [2]. A dedicated folding machine applied a moment by pushing perpendicularly to the loaded panel (F0) during the rotation (Figure 4). The orientation of the sample in the machine determined whether the angle between the two panels was reduced (closing, Figure 4a) or increased (opening, Figure 4b) during the deformation. The deformation was measured by averaging measurements

2

from two inclinometers, and the load by summing two load cell responses.
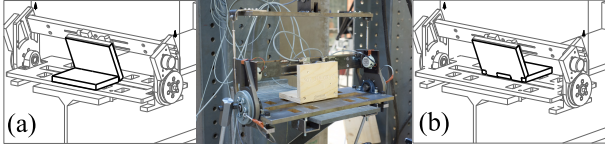
Figure 4: *Folding machine: (a) closing and (b) opening.*

Five replicates of each geometry were tested in opening and closing (Figures 4a,4b), giving a total of 80 results.

3.2 RESULTS

The experimental results are represented as non-linear average moment–rotation curves (Figures 5 and 6). The linear part fits between 10% and 40% of the ultimate moment in each case. Tables 1 and 2 present the values of average stiffness and ultimate moment for each sample (from five replicates) in the two directions of loading. The MTSJ with closed slots and TTs (sample (g)) was more than twice as stiff and twice as strong as the screwed connection (sample (h)) in closing. Combining DJ or FJ with crossing screws improved the stiffness of the connections asymmetrically. Screwed connections generally show a significant difference of stiffness between closing and opening owing to the rig effect described in Ref. [2] combined with the screw pressing effect. In Figure 2, the red contact surfaces of samples (c) and (d) are pre-stressed by the screwing. These surfaces are then fully carried with limited slip during the opening of the joint. In closing, the screw heads are pulled out, and only the threads resist comparatively weakly against the induced tension.

Figure 7 shows the symmetric behavior of the MTSJ-TT for both loading directions. The elastic part of the curves ends after a very limited rotation of less than 5°. The next section focuses on the embedment volume geometry of this particular type of MTSJ.

4 EMBEDMENT EFFECT ON MTSJ WITH TT

4.1 CONTACT SURFACES

After testing, sample (g) was cut and scanned to identify the contact surface and the geometry of the deformed volumes (Figure 8). As the behavior is symmetric, Figure 9 presents only the embedment effect in closing. Where the tenons go through the slots, an embedment zone is present at each side of the tab faces (DC, Figure 9a). It results in a self-locking effect. In addition, the shoulders of the F_0 panel compressed the surface of the F_1 panel, leading to a single deformation on the bottom face F_{1-} (SC, Figure 9b). The internal local forces at each deformed zone counterbalance the external bending moment. The total resisting moment of the joint is obtained by multiplying each local force by its respective lever arm measured from the rotation center of the joint. This study is limited to the geometry of the deformed volumes, from which the local

Table 3: *Sample parameters for partial compression*

Parameters	Symb.	Unit	a	b	c	d	e	f
Joint length	JL	mm	50	50	50	50	30	30
Panel thickness	t	mm	21	21	21	21	21	21
Standing panel	SP	-	S	K	K	S	K	S
Lying panel	LP	-	K	K	K	K	K	K
Edge distance	ED	mm	0	0	63	63	50	50
Tab protrusion	P	mm	-	-	-	-	10.5	10.5
Replicate	-	-	8	8	4	1	5	5

K = LVL Kerto-Q, S = Steel

forces can be determined by using Equation (2).

$$P_\theta = \frac{V_\theta}{t} \cdot E_\theta \quad \text{with} \quad E_\theta = \frac{E_{90,edge,mean} \cdot E_{90,flat,mean}}{E_{90,edge,mean}\sin^{1.8}\theta + E_{90,flat,mean}\cos^{1.8}\theta} \quad (2)$$

Here, P_θ, V_θ, t, and E_θ are the local force, the embedded volume, the reference thickness (here $t = t_0 = t_1$), and the elastic modulus of LVL Kerto-Q at θ angle, respectively. Inspection of the surfaces also confirmed the exponential form of the indirectly loaded surfaces, as analyzed by Japanese researchers [8][10][11]. Additional experiments formalized the mechanical behavior of the embedment and the decay coefficients.

4.2 EMBEDMENT BY ROTATIONAL PARTIAL COMPRESSION

4.2.1 Description of the tests

The test comprised two parts: the first characterized the mechanical behavior of the MTSJ in partial compression with rotation, and the second analyzed the additional length profile. As described in the previous section, a MTSJ shows two types of rotational compression, SC and DC. Both phenomena were studied here. For each test, six series of samples with different geometries and with wood and steel matrices for the standing panel (SP) were tested (Figure 10). The geometric properties and characteristics of each sample are listed in Table 3.

Samples were tested using a setup designed for partial compression with rotation (Figure 11). A 20 kN cylinder pressing on a steel lever arm was used to transmit rotation θ on the SP, which bore the surface of the lying panel (LP). The lever arm kept the load perpendicular to the standing panel in any position. The LP was rigidly fixed by a steel clamp. The location of the rotation center could be set depending on the geometry of the test sample. Rotation and load were recorded by two inclinometers and the cell load. A total of 31 specimens were tested. All these tests were performed with the grain parallel to the length of the joint with a dihedral angle equal to 90°.

4.2.2 Moment–rotation behavior in partial compression

All the tests explored the mechanical behavior of this joint in partial compression with rotation angles from 0°to 25°(Figure 12). First, the clearance of the joint caused an initial displacement, and special attention was given to the production of the samples to minimize it. This deformation is an essential consideration in structure design, and receives particular attention in the current European standards. Secondly, the joint stiffness was
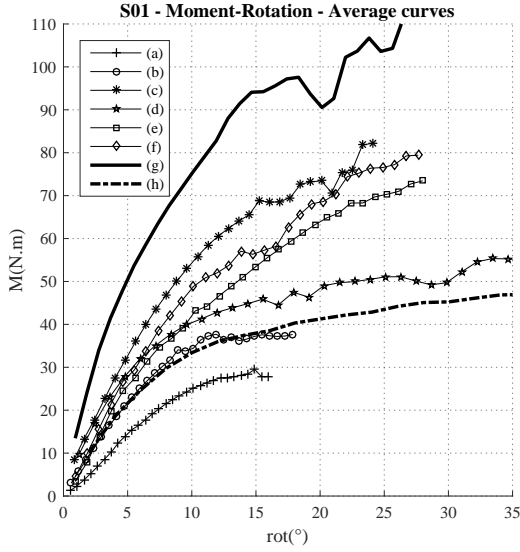
3

Figure 5: *S01 (closing): moment–rotation curves up to the maximum point.*
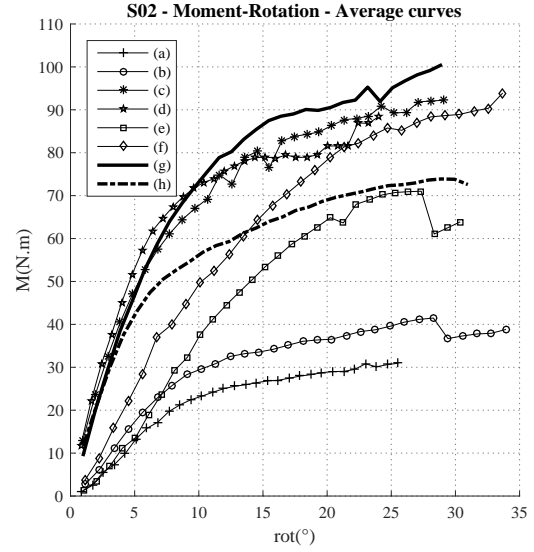

Figure 6: *S02 (opening): moment–rotation curves up to the maximum point.*

Table 1: *Average stiffness and ultimate moment for S01*

| Sample | Type | θ_1-θ_2-θ_3 | Moment max. | | Stiffness | |
			Mean N·m	Std. -	Mean N·m/°	Std. -
a	(JJ)	00-00-30	28	2.5	3.1	0.2
b	(DJ)	00-00-30	37	4.2	4.5	0.1
c	(DJ+S)	00-00-30	72	7.2	6.3	0.2
d	(FJ+S)	00-00-00	53	5.0	5.8	0.9
e	(2SF)	00-00-00	70	4.4	5.1	0.2
f	(1SF)	00-00-00	76	5.7	5.9	0.7
g	(TT)	00-00-00	106	10.6	9.9	0.8
h	(S)	3xscrew4.5	49	1.6	4.3	0.07

Table 2: *Average stiffness and ultimate moment for S02*

| Sample | Type | θ_1-θ_2-θ_3 | Moment max. | | Stiffness | |
			Mean N·m	Std. -	Mean N·m/°	Std. -
a	(JJ)	00-00-30	31	2.7	3.2	0.6
b	(DJ)	00-00-30	42	3.4	4.0	0.6
c	(DJ+S)	00-00-30	84	13.3	10.5	1.1
d	(FJ+S)	00-00-00	82	6.2	10.8	1.0
e	(2SF)	00-00-00	71	5.8	4.9	0.4
f	(1SF)	00-00-00	86	7.5	5.5	0.7
g	(TT)	00-00-00	95	5.6	9.4	0.9
h	(S)	3xscrew4.5	74	1.0	9.0	0.12

Figure 7: *Symmetrical behavior of TT.*

Figure 8: *Scan of F_{0+} embedment area with a FaroArm.*

average of all the replicates of each sample was taken, so only average curves are displayed in the figures.

Wood's anisotropic properties mean that its elastic modulus changes with its grain orientation. The use of a steel punch avoided parasitic effects due to the edge deformation of the standing panel after a certain rotation angle. Nevertheless, some tests were also conducted with a wood punch to reproduce the actual behavior of the joint. The mechanical behavior of the joint was more homogeneous with the steel punch (Figure 13): its standard deviation with a wood punch was almost 4 times larger than that with a steel one. As a result, the SP distortion at the corner of the contact surface was not negligible, and could be considered in the theoretical
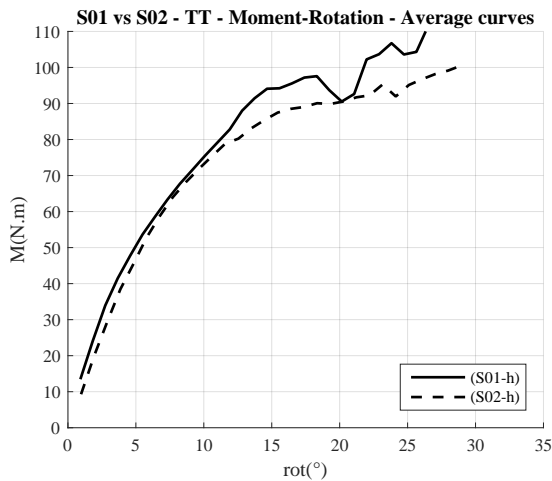
determined in the elastic region by a linear regression from 0.1 to 0.4 $M_{u,D}$. The yield point was defined as the intersection of the elastic and the plastic regression lines. Densification was not achieved, because the rotation angle should have been much larger; however, a joint with such a large strain is structurally useless. As a consequence of the setup limitation, the maximum moment observed in the test was not the real ultimate moment of the joint. An
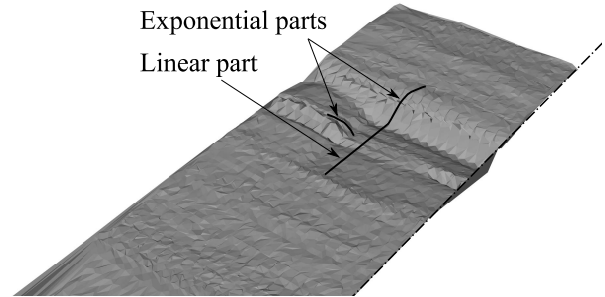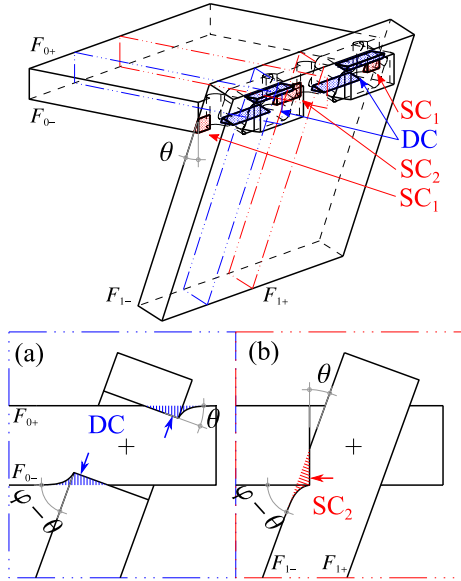
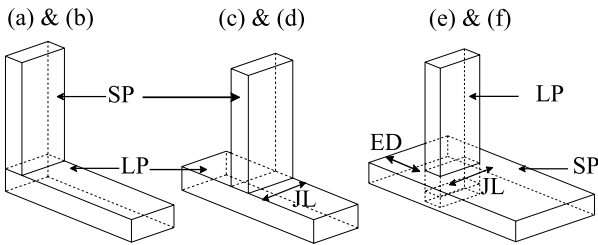**Figure 9:** *Embedment effect in MTSJ-TT: (a) DC and (b) SC.*

Figure 10: *Sample geometries.*

estimation of mechanical performance. The Hankinson empirical formulas can help to characterize the elastic modulus in different orientations [13].

All the stiffness and the yield point results are listed in Table 4. The curves are presented for SC and DC (Figures 14 and 15). Using the steel punch gave higher results than those from using wood for the reasons described above. For SC, when the edge distance was 63 mm, the elastic stiffness increased by 21% compared with no edge distance. The increase did not affect the yield moment. Further tests will be conducted to characterize the stiffness with respect to this distance.
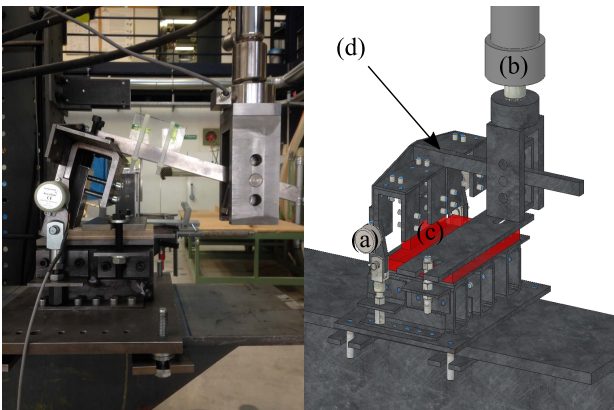

Figure 11: *Rotational partial compression setup: (a) 2x inclinometers, (b) cylinder and 20kN cell loads, (c) sample, and (d) lever arm.*
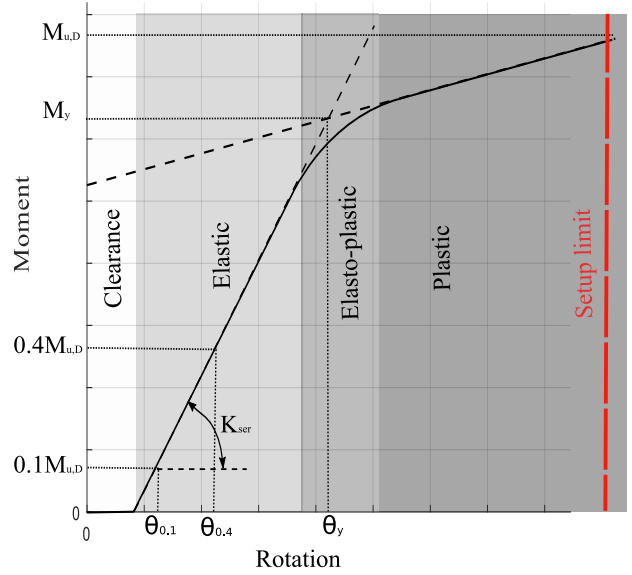

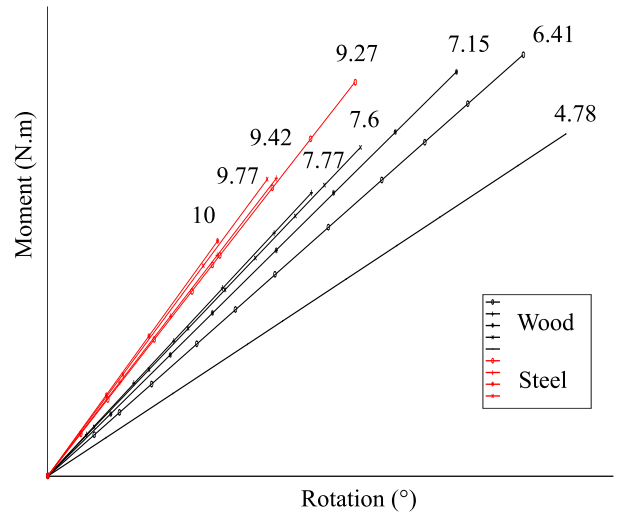**Figure 12:** *Mechanical behavior in rotational partial compression.*

Figure 13: *Corresponding stiffness with steel or Kerto Q punch.*

Table 4: *Elasto-plastic values for partial rotational compression*

Sample	Elastic stiffness (N·m/°)	Plastic stiffness (N·m/°)	Yield moment (N·m)	Yield rotation (°)
a	10.9	4.6	99.2	7.5
b	12.1	4.1	64.7	4.6
c	15.1	4.4	69.5	4.1
d	14.1	6.3	92.3	5.6
e	6.1	3.1	38.0	6.1
f	9.5	2.6	47.1	5.1

Table 5 gives a comparative analysis of the SC and DC joints. The joint length is 40% lower in the DC configuration than in the SC one. Given that the mechanical strength is proportional to the joint length, the yield rotation behavior is not similar in both configurations. Based on these results, the mechanical performances of the SC and the DC configurations are largely quasi equal. The exception is the yield moment, which is more important in the DC configuration
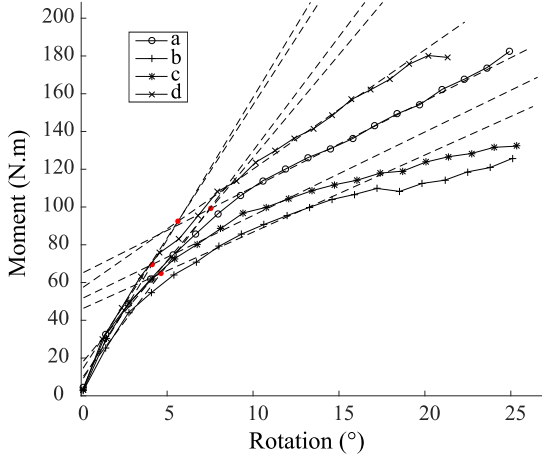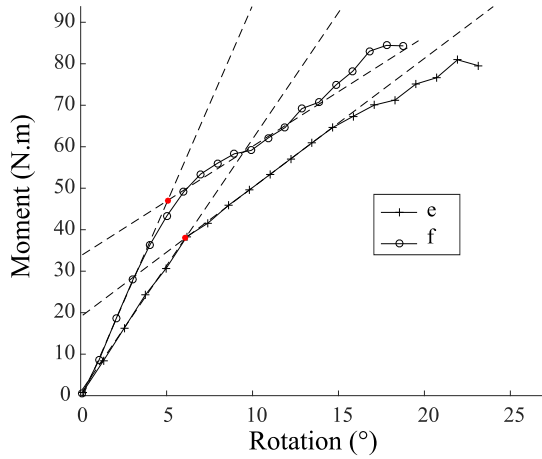
Figure 14: *SC moment–rotation curves.*

Figure 15: *Double contact moment–rotation curves.*

according to the proportionality of this test. A setup with a higher rotation range could refine the linear regression in the plastic part, and thus provide a more accurate yield point. In the current setup, the MTSJ showed homogeneous behavior in its different loaded areas, leading to the stress distributing uniformly in the joint and so avoiding failure at a singular weak point.

Table 5: *Comparison of SC and DC*

Contact	Elastic stiffness (N·m/°)	Plastic stiffness (N·m/°)	Yield moment (N·m)	Yield rotation (°)	Joint length mm
SC	13.1	4.9	81.5	5.5	50
DC	7.8	2.9	42.5	5.6	30
≠	40 %	41 %	48 %	2 %	40 %

4.2.3 Analysis of the additional length profile

The additional length takes the form of an exponential curve whose shape is determined by the γ coefficient, which needs to be set according to the different geometries of the MTSJs.

The rotation angle and strain are both small in the elastic

part. For this reason, the additional length was studied only in the plastic part (Figure 16). The deformations were monitored with a high-resolution camera during the experiment. Afterwards, the final deformations were scanned with a FaroArm to compare the data processing from the camera pictures (Table 6). The results from both data processes appeared almost equal, with a difference of just 0.5%. The reliability of the data processes was therefore verified.
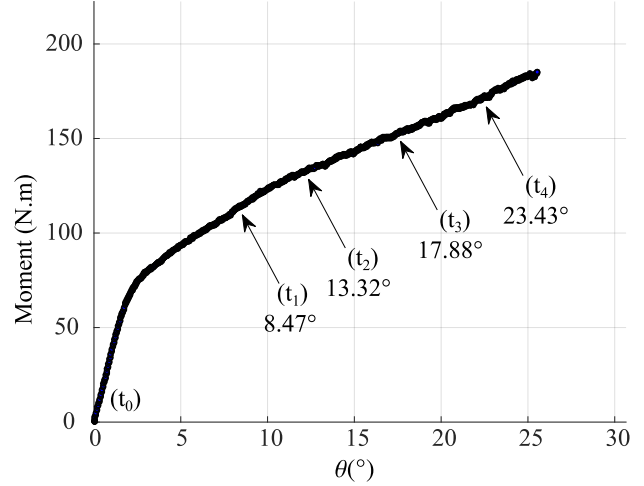

Figure 16: *Selected times on the moment–rotation curve.*

Table 6: *Comparative fit of γ coefficient - Scan vs camera*

Type	Scan	Camera
ID Time	t4	t4
Time(s)	600	600
γ	0.4407	0.4432
Adj. Rsquare	0.96	0.99
Nb. curves	7	5

First, the effect of geometry on the γ coefficient was studied (for the same 25°rotation angle). All the γ coefficients for the different geometries are listed in Table 7. The additional length of sample (d) was not studied owing to the lack of consistent values from the few specimens available. Table 8 compares the values between SC and DC. The additional length in the DC was small, which may account for most of the disparity in the results. The γ coefficient for the DC was 77% bigger than that for the SC. As a result, the additional length was less important in the DC area of the joint for a given rotation angle.

Table 7: *γ coefficient at 25°of rotation*

Sample	a	b	c	d	e	f
γ_{min}	0.27	0.22	0.15	-	1.77	1.11
γ_{max}	1.14	1.34	0.89	-	4.51	3.58
γ_{mean}	0.50	0.53	0.55	-	2.95	1.76
SD	0.21	0.28	0.24	-	0.88	0.95
Adj. Rsquare	0.95	0.97	0.95	-	0.94	0.93
Nb.samples	8	8	4	-	5	5
Nb.curves	21	25	10	-	12	6

Table 8: *γ coefficients for SC or DC*

Sample	SC	DC
γ_{min}	0.21	1.44
γ_{max}	1.12	4.04
γ_{mean}	0.53	2.35
SD	0.24	0.91
Adj. Rsquare	0.96	0.93
Nb.samples	7	5
Nb.curves	19	9

Table 9: *Evolution of γ with rotation steps*

Time step	t_1	t_2	t_3	t_4
Time(s)	240	360	480	600
$\theta(°)$	8.47	13.32	17.88	23.43
γ	0.638	0.578	0.500	0.443
SD	0.06	0.07	0.06	0.06
Adj. Rsquare	0.99	0.98	0.99	0.99
δ**(mm)**	1.96	3.03	4.17	5.14
Strain (%)	9.6	14.7	20	25

In the second step, the evolution of the additional length was studied using time-lapse photography (Figure 17). Sample (a) is shown with a fixed interval of 120 seconds between each picture. Figure 18a displays the area of additional length with respect to different angles of rotation.
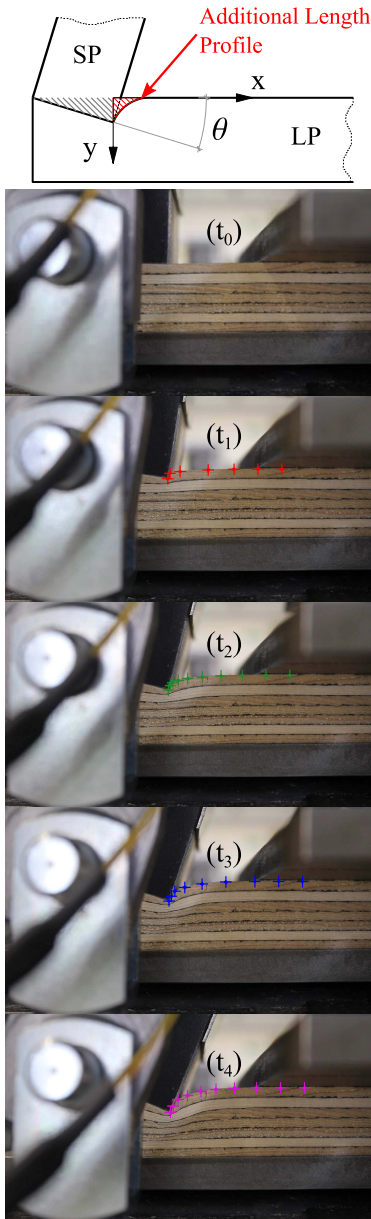
Figure 17: *Time-lapse photographs of the displacement profile.*

The shape of the exponential curve varied with the angle of rotation, although there was a linear correlation

between the γ coefficient and the strain of the LP in this configuration (Figure 18b and Table 9). The larger the rotation, the smaller the γ coefficient was.

The effect of this coefficient was understood and observed at a given rotation angle (time=t_4, $\theta = 23.43°$): the higher the γ coefficient, the smaller the additional length was (Figure 18c). However, the additional length represented a small part of the total deformed area. Considering a constant γ coefficient during the rotation of the joint, the average error was only 3.5%. A uniform value of γ could be used with little effect on the result.

4.2.4 Embedded volumes

The total deformed volume due to the rotational partial compression can be divided into elementary volumes (V_i, Figure 19). Each volume is described by the following integrations (Equations (3) to (8)), which are expressed with the geometrical parameters of the directly and indirectly loaded area given in Figure 3 and Table 10.

$$V_1 = \frac{1}{2} \cdot w_1 \cdot l_1 \cdot h_1 \tag{3}$$

$$V_2 = \int_0^{l_1} \int_0^{w_2} x \cdot \tan\theta \cdot \exp(-\gamma y) \, dy \, dx \tag{4}$$

$$V_3 = \int_0^{l_1} \int_0^{w_3} x \cdot \tan\theta \cdot \exp(\gamma(y - w_3)) \, dy \, dx \tag{5}$$

$$V_4 = w_1 \cdot \int_0^{l_4} h_1 \cdot \exp(-\gamma x) \, dx \tag{6}$$

$$V_5 = \int_0^{l_4} \int_0^{w_3} h_1 \cdot \exp(-\gamma x) \cdot \exp(\gamma(y - w_3)) \, dy \, dx \tag{7}$$

$$V_6 = \int_0^{l_4} \int_0^{w_2} h_1 \cdot \exp(-\gamma x) \cdot \exp(-\gamma y) \, dy \, dx \tag{8}$$

Table 10: *Embedded volume parameter values*

| Param.	SC1 Name	Value	SC2 Name	Value	DC* Name	Value
w_1	$M_{sh,end}$	13	M_{sh}	26	L_{se}	37.2
w_2	-	0	N_{r0}	12	N_{r1}	6.4
w_3	N_{r0}	12	N_{r0}	12	N_{r1}	6.4
l_1	$L_{\theta,SC}\cos\theta$	-	$L_{\theta,SC}\cos\theta$	-	$L_{\theta,DC}\cos\theta$	-
l_4	$P_{22}+$	139.5	P_{22}	139.5	P_{01}	10.7
					(P_{02})	(139.5)
h_1	$L_{\theta,SC}\sin\theta$	-	$L_{\theta,SC}\sin\theta$	-	$L_{\theta,DC}\sin\theta$	-
γ	γ_{SC}	0.53	γ_{SC}	0.53	γ_{DC}	2.35

* For each of the two embedded volumes, P_{01} and P_{02} set the l_4 value, respectively.

The length of the directly loaded surface is $L_{\theta,k} = t/2(1 + \tan\theta/2) - C/\tan\theta$, where t is the panel thickness and C is the clearance between the tab and slot.

The plastic range is reached quickly during the deformation. If we consider that δ_y is the point where
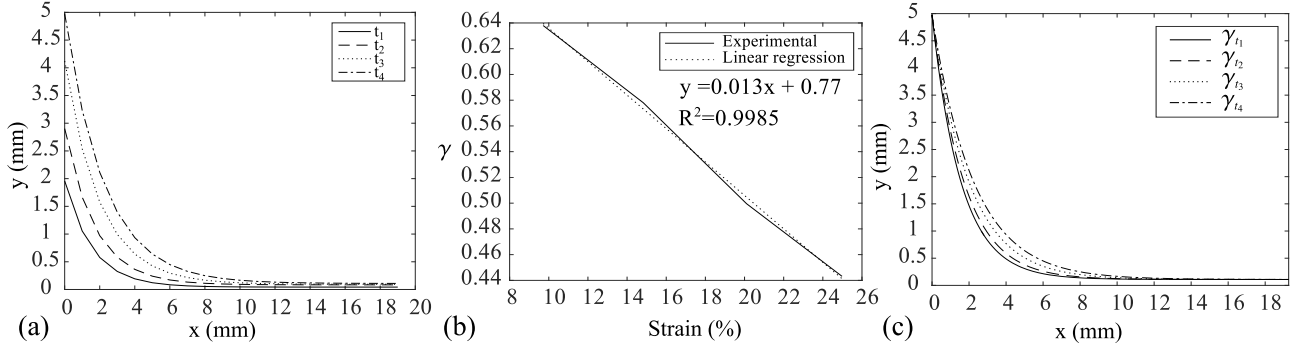
Figure 18: *γ coefficients: (a) at each step t_i, (b) linear regression of $\gamma = f(strain)$, and (c) comparison with t_4 displacement*

(a)

(b)
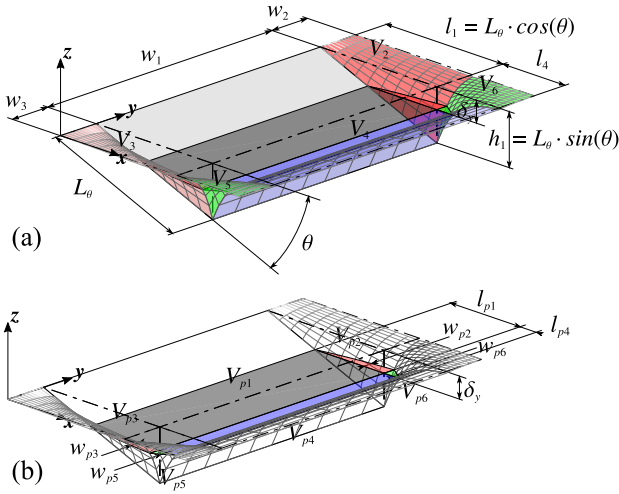
Figure 19: *(a) Elasto-plastic deformed volumes. (b) Details after yield point.*

the plastic deformation starts, then the elementary plastic volumes are defined by Equations (9) to (14).

$$V_{p_1} = \frac{1}{2} \cdot w_1 \cdot l_{p_1} \cdot (h_1 - \delta_y) \tag{9}$$

$$V_{p_2} = \int_{l_1-l_{p_1}}^{l_1} \int_0^{w_{p_2}} (x \cdot \tan\theta \cdot \exp(-\gamma y) - \delta y) dy dx \tag{10}$$

$$V_{p_3} = \int_{l_1-l_{p_1}}^{l_1} \int_0^{w_{p_3}} (x \cdot \tan\theta \cdot \exp(\gamma(y-w_3)) - \delta y) dy dx \tag{11}$$

$$V_{p_4} = w_1 \cdot \int_0^{l_{p_4}} (h_1 \cdot \exp(-\gamma x) - \delta y) dx \tag{12}$$

$$V_{p_5} = \int_0^{l_{p_4}} \int_0^{w_{p_5}} (h_1 \cdot \exp(-\gamma x) \cdot \exp(\gamma(y-w_3)) - \delta y) dy dx \tag{13}$$

$$V_{p_6} = \int_0^{l_{p_4}} \int_0^{w_{p_6}} (h_1 \cdot \exp(-\gamma x) \cdot \exp(-\gamma y) - \delta y) dy dx \tag{14}$$

with

$$l_{p_1} = l_1 - \frac{\delta y}{\tan\theta} \tag{15}$$

$$w_{p_2} = -\frac{1}{\gamma} \ln\frac{\delta y}{x\tan\theta} \quad \text{with} \quad l_1 - l_{p1} \le x \le l_1 \tag{16}$$

$$w_{p_3} = \frac{1}{\gamma} \ln\frac{\delta y}{x\tan\theta} + w_3 \quad \text{with} \quad l_1 - l_{p1} \le x \le l_1 \tag{17}$$

$$l_{p_4} = -\frac{1}{\gamma} \ln\frac{\delta y}{h_1} \tag{18}$$

$$w_{p_5} = \frac{1}{\gamma} \ln\frac{\delta y}{h_1 * \exp(-\gamma x)} + w_3 \quad \text{with} \quad l_1 - l_{p1} \le x \le l_1 \tag{19}$$

$$w_{p_6} = -\frac{1}{\gamma} \ln\frac{\delta y}{h_1 * \exp(-\gamma x)} \quad \text{with} \quad l_1 - l_{p1} \le x \le l_1 \tag{20}$$

The elastic embedded volumes are obtained by

$$V_{e_i} = V_i - V_{p_i}.$$

5   CONCLUSIONS

The rotational stiffness of an edge-to-edge connection of a timber folded-plate structure was increased by using a TT and closed slots. The effect of embedment, which provided strength, stiffness, and ductility to the connection, was identified and explained. Quantitative analysis provided values for the decay coefficients of the additional length curves in single and double contact. The embedded volumes were analytically described. Their use in the description of the local forces will allow subsequent work to formulate an analytical model of the MTSJ rotational behavior. Further works will aim to determine the γ coefficient with respect to the material properties (LVL), panel thickness, grain orientation, protrusion lengths, dihedral angle φ, tab number, and types of contact. This paper demonstrates that a MTSJ with TT performs better under a bending moment than a screwed angular connection for thin LVL panels.

REFERENCES

[1] Robeller C., Stitic A., Mayencourt P. and Weinand Y.: Interlocking Folded Plate – Integrated Mechanical Attachment for Structural Wood Panels. In: AAG, London, U.K., Springer, 2014.

[2] Roche S., Mattoni G. and Weinand Y.: Rotational Stiffness at Ridges of Timber Folded-plate Structures. International Journal of Space Structures, Vol. 30, N°2, 153-167, 2015.

[3] Krieg O. D., Schwinn T., Menges A., Li J-M., Knippers J., Schmitt A. and Schwieger V.: Biomimetic Lightweight Timber Plate Shells: Computational Integration of Robotic Fabrication, Architectural Geometry and Structural Design. In: AAG, London, U.K., Springer, 2014.

[4] Robeller C. and Weinand Y.: Fabrication-aware Design of Timber Folded Plate Shells with Double Through Tenon Joints. In: Robotic Fabrication in Architecture, Art and Design 2016, Springer, 2016.

[5] Chang W.-S., Hsu M.-F., Komatsu K. : Rotational Performance of Traditional Nuki Joints with Gap I :

Theory and Verification. Journal of Wood Science, ol. 52, No. 1, 58-62, 2006.

[6] Tanahashi H. and Suzuki Y.: Embedment Mechanism and Formulation of Major Types of Traditional Wooden Joints in Japan. In: World Conference on Earthquake Engineering, Lisbon, Portugal, 2012.

[7] Ogawa K., Sasaki Y., Yamasaki M. : Theoretical Modeling and Experimental Study of Japanese "Watari-ago" Joints. Journal of Wood Science, Vol. 61, No. 5, 481-491, Springer Japan, 2015.

[8] Inayama M.: Study on Compression Perpendicular to the Grain in Wood. Part 4: Analytic Functions for the Relation between Compression Load and Elastic Deformation Perpendicular to the Grain in Wood. In: Proceedings of AIJ, Tokyo, 1993.

[9] Tanahashi H., Okamura M., Suzuki Y.: Simple Formulation of Elasto-Plastic Embedment Behavior of Orthotropic Wood Considering Densification. WCTE 2008.

[10] Kitamori A., Mori T., Katoaka Y., Komatsu K.: Effect of Additional Length on Partial Compression Perpendicular to the Grain of Wood. J. Struct. Constr. Eng., AIJ, Vol. 74, No. 642, 1477-1485, August 2009.

[11] Matsubara Y., Du Z., Sakata H., Wada A., Ito H., Kataoka R.: Experimental Study on the Behavior of Rotational Embedment. Summaries of Technical Papers of Annual Meeting, AIJ, 2002.

[12] Robeller C., Mayencourt P., Weinand Y. : Snap-fit Joints - CNC fabricated, Integrated Mechanical Attachment for Structural Wood Panels. ACADIA 2014, 34th Annual Conference of the Association for Computer Aided Design in Architecture, Los Angeles, California, USA, October 23-25, 2014.

[13] Hankinson R. L. : Investigation of Crushing Strength of Spruce at Varying Angles of Grain. Air Force Information Circular No. 259, 1921.